The role of ABCA1 on glomerular lipid accumulation and renal injury in focal segmental glomerulosclerosis

Jimin Park

Department of Medical Science

The Graduate School, Yonsei University

The role of ABCA1 on glomerular lipid accumulation and renal injury in focal segmental glomerulosclerosis

Directed by Professor Shin-Wook Kang

The Doctoral Dissertation
submitted to the Department of Medicine,
the Yonsei University Graduate School of Medicine
in partial fulfillment of the requirements for the degree of
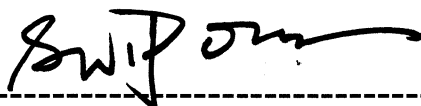Doctor of Philosophy

Jimin Park

December 2021

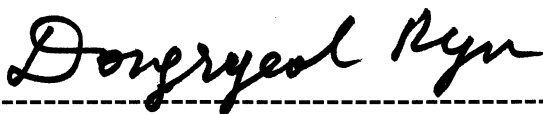This certifies that the Doctoral Dissertation
of Jimin Park is approved.

Thesis Supervisor: Shin–Wook Kang

Thesis Committee Member #1: Tae–Hyun Yoo

Thesis Committee Member #2: Sahng Wook Park

Thesis Committee Member #3: Heon Yung Gee

Thesis Committee Member #4: Dong-Ryeol Ryu

The Graduate School
Yonsei University

December 2021

TABLE OF CONTENTS

LIST OF FIGURES

LIST OF TABLES

The role of ABCA1 on glomerular lipid accumulation and renal injury in focal segmental glomerulosclerosis

Jimin Park

Department of Medical Science
The Graduate School, Yonsei University

(Directed by Professor Shin-Wook Kang)

Glomerular lipid accumulation is one of the pathologic characteristics of focal segmental glomerulosclerosis (FSGS). Recent evidence suggests that ATP-binding cassette transporter A1 (ABCA1) has effects on the cellular lipid homeostasis. This study aimed to evaluate the role of ABCA1 on lipid accumulation in glomeruli and podocyte under FSGS conditions.

Using human kidney biopsy samples, the expression of the *Abca1* mRNA was analyzed in glomeruli in patients with FSGS. *In vitro*, mouse podocytes were stimulated with adriamycin (ADR) and TNF-α, and these cells were also co-treated with GW683965, an LXR-α agonist to upregulate ABCA1 expression. *In vivo*, C57BL/6 and podocyte-specific *Abca1* knockout mice were administered intravenously with ADR at 25 mg/kg. GW683965 (1 mg/kg/day) was treated via osmotic pumps (10mg/kg/ in ADR-treated BALB/c mice. The levels of albumin in urine, and the levels of cholesterol, and triglyceride in kidney tissues were measured in animals. Active RhoA staining and Bodipy 493/503 staining for glomerular cholesterol assay were performed. Apoptosis- and mitochondrial injury-related markers were evaluated both *in vitro* and in *vivo*.

Compared to the control group, the levels of albumin in urine, and the levels of cholesterol and triglyceride in the glomeruli were significantly increased and

effacement of foot processes assessed by transmission electron microscopy was observed in ADR-induced FSGS mice. These changes were aggravated in podocyte-specific *Abca1* knockout FSGS mice, while they were abrogated by GW683965 via upregulation of glomerular ABCA1 expression. The cholesterol and triglyceride contents in kidneys were higher in FSGS models, and were reduced by GW683965. Mitochondrial morphology and the metabolic enzymes were highly deranged in the kidneys of ADR-treated podocyte-specific *Abca1* knockout mice. These mitochondrial abnormalities in the FSGS models were improved by replenishing ABCA1 with GW683965 treatment. *In vitro*, the intracellular lipid contents were increased and subsequent apoptosis and mitochondrial dysfunction were also increased in podocytes treated with ADR and TNF-α. Cellular lipid accumulation and mitochondrial injury by ADR and TNF-α stimuli were ameliorated through GW683965 treatment as an ABCA1 enhancer.

The role of ABCA1 on glomerular lipid accumulation and renal injury in focal segmental glomerulosclerosis

Jimin Park

Department of Medical Science
The Graduate School, Yonsei University

(Directed by Professor Shin-Wook Kang)

I. INTRODUCTION

Worldwide, focal segmental glomerulosclerosis (FSGS) is the most common primary glomerulonephritis and progresses to ESRD frequently.[1] FSGS patients show the podocyte injury and proteinuria, and subsequent develop glomerulosclorosis.[2] Pathologic findings demonstrate that FSGS is characterized by cholesterol accumulation and cellular apoptosis in glomeruli.

Cholesterol is a major component of cell membrane and it is essential for cell survival.[3] However, excessive accumulation of cholesterol within the cell causes toxic effects such as mitochondrial dysfunction and consequent apoptosis. Intracellular cholesterol is regulated by cholesterol influx, *de novo* cholesterol synthesis, and efflux.[4] Almost animal cells synthesize the cholesterol by acetyl-coenzyme A.[5] In addition, circulating cholesterol enters into cells, mediating by binding to low density lipoprotein (LDL) receptors within the cellular membrane.[6] Intracellular cholesterol is actively transported to extracellular space by ATP-binding cassette transporters A1 (ABCA1) or ATP-binding cassette transporters G1 (ABCG1) and binds with high-density lipoprotein.[7] The

abnormalities in this process induce the intracellular cholesterol accumulation and cause cytotoxic effects in various disease models.[8,9] As recent reports have shown, the downregulation of the ABCA1 causes an accumulation of intracellular cholesterol and increases in the apoptosis of podocyte in animals with diabetic kidney disease (DKD).[10-12] Previous studies demonstrated that glomerular ABCA1 in FSGS patients has also been down-regulated and negatively associated with atherosclerosis.[13,14] In addition, the amount of albuminuria in TNF-α stimulated mice was exacerbated by podocyte-specific *Abca1* deficiency and partially prevented by ABCA1 overexpression.[15] However, there was still a lack of evidence of ABCA1 affecting regulation of cholesterol metabolism and podocyte damages in the focal segmental glomerulosclerosis (FSGS) model.

Therefore, I planned to investigate the role of ABCA1 in regulating the cholesterol metabolism on podocyte and the effect of cholesterol accumulation on podocyte damage in an experimental FSGS model.

II. MATERIALS AND METHODS

1. Human study

The human kidney samples and demographic data were obtained from the Yonsei Renal cDNA Bank. The biopsy kidney specimens were manually micro–dissected and glomeruli were isolated,[16,17] and glomerular mRNA expression profiling was performed as previously described.[18] Totals of 113 samples, 43 samples, and 50 samples were confirmed with focal segmental glomerulosclerosis (FSGS) and IgA nephropathy (IgAN), respectively, while 20 samples of normal kidney as confirmed pathologically were used as a control group. The biochemical data for each sample were also obtained from medical records. Informed consents were obtained from all patients. This study was approved by the Institutional Review Board of the Yonsei University Health System Clinical Trial Center (IRB No. 4-2019-0548).

2. Animal study

To generate podocyte-specific *Abca1* knockout mouse, podocin-Cre transgenic mice with a genetic background of C57BL/6J (cat no. 008205) and Abca1 flox/flox mice with C57BL/6J genetic background (cat no. 028266) were purchased from Jackson Laboratory (Bar Harbor, ME, USA). Then, I bred *Abca1* flox/flox mice with podocin-Cre transgenic mice. I identified transgenic mice by genotyping from tail DNA preparations with polymerase chain reaction. The mice were maintained in a temperature- and humidity-controlled environment with a 12-h light-dark cycle.

Previous study reported that BALB/C mice is a suitable model for FSGS by ADR, but C57BL6 mice is resistant to ADR. Therefore, I used two FSGS model for the experiment. To generate the FSGS animal model, C57BL/6 and podocyte-specific *Abca1* knockdown mice, aged 6 weeks, were administered with intraperitoneal injections of adriamycin at 25 mg/kg of body weight. In addition,

BALB/c mice were treated with 10.5mg/kg of ADR and GW683965 (1 mg/kg/day) which is an LXR-α agonist upregulating the expression of ABCA1 was implanted via osmotic pumps in ADR-treated BALB/c mice.

Mice in different groups were used so that metabolic cage analysis could be performed. They were sacrificed through the direct collection of blood from the heart and the perfusing with saline. Following immediate centrifugation at 4°C, plasma was separated and stored at -20°C until analysis, and kidney tissues were also collected.

All animal studies were performed in accordance with the guidelines of the National Institutes of Health (IACUC No. 2017-0335).

3. Cell culture studies

Conditionally immortalized mouse podocytes were kindly provided by Dr. Peter Mundel (Harvard Medical School and Massachusetts General Hospital, Boston, MA, USA) and were cultured as previously described.[19] Briefly, frozen podocytes were first grown under permissive conditions at 33°C in RPMI-1640 medium (Sigma, Saint Lousis, MO, USA) containing 10% fetal bovine serum (FBS, Gibco, Grand Island, NY, USA), 10 U/mL interferon-γ (INF-γ, Sigma), and 100 U/mL of penicillin/streptomycin (Gibco) in collagen-coated flasks, and the INF-γ was incrementally reduced to 10 U/mL in successive passages. The cells were then trypsinized and subcultured without INF-γ (non-permissive conditions) and were allowed to differentiate at 37°C with the medium changed on alternate days.

Differentiation of the podocytes grown for 14 days at 37°C was confirmed by the identification of synaptopodin, a podocyte differentiation marker, by reverse transcription polymerase chain reaction (RT-PCR) and Western blotting. After confirming the differentiation of podocytes and serum restriction for 24 h, the medium was changed to serum-free RPMI medium containing TNF-α (5 ng/ml) and ADR (0.125 ug/ml) with or without GW683965 (1 uM).

4. Total RNA extraction

Total RNA was extracted from mouse kidney as previously described.[20] Briefly, the samples of the whole kidney were rapidly frozen using liquid nitrogen and homogenized by mortar and pestle thrice with 700 μL of RNA STAT–60 reagent (TaKaRa, CA, USA). After homogenizing the suspension for 5 min at room temperature, 160 μL of chloroform was added. Next, the mixture was shaken vigorously for 30 sec, incubated for 10 min in ice, and centrifuged at 12,000 ×g for 15 min at 4°C. The upper aqueous phase containing the extracted RNA was transferred to a new tube. RNA was precipitated from the aqueous phase by adding 400 μL of isopropanol, and then pelleted by centrifugation at 12,000 ×g for 30 min at 4°C. The RNA precipitate was washed with 70% ice–cold ethanol, air dried for 10 min, and dissolved in diethyl pyrocarbonate (DEPC)–treated distilled water. The RNA yield and quality were assessed based on spectrophotometric measurements at wavelengths of 260 and 280 nm. Total RNAs from cultured podocyte cells were extracted similarly.

5. RNA-Seq and gene expression analysis

Affected genes were screened in ADR-treated FSGS mice and the control. After isolation of glomeruli, RNA was extracted in the glomeruli. A total amount of 2 μg RNA per sample was used as input material for the RNA sample preparations. Sequencing libraries were built using the NEBNext® Ultra™ RNA Library Prep kit of Illumina® (cat. no. E7530L; New England Biolabs, Inc., Hitchin, England) following the manufacturer's instructions, and index codes were added to attribute sequences to each sample. Based on the manufacturer's instructions, the index-coded samples were clustered on a cBot cluster generation system using the HiSeq PE Cluster kit v4-cBot-HS (Illumina, Inc., San Diego, CA). After the cluster had been generated, the libraries were sorted on an Illumina platform to generate 150 bp paired-end reads. Genes with a false discovery rate (FDR) <0.1 and fold-change (FC) >2 were identified as DEGs. Data analysis and pathway

enrichment analysis were performed using integrated Differential Expression and Pathway analysis (iDEP, version 0.90; http://ge-lab.org/idep).[21] iDEP is an online application that integrates many Bioconductor packages and annotated databases to enable users to perform intensive bioinformatics analysis. In the present study, the DESeq2 package, hierarchical clustering and κ-means clustering analysis, principal component analysis, Gene Ontology (GO) analysis, transcription factor binding motifs and microRNA enrichment analysis were used in the iDEP application.

6. Reverse transcription

A Takara cDNA synthesis kit (Takara Bio Inc., Otsu, Japan) was used to obtain the first stand cDNA. Two micrograms of total RNA extracted from tissues and cultured cells were reverse transcribed using a 10 μM random hexanucleotide primer, 1 mM dNTP, 8 mM $MgCl_2$, 30 mM KCl, 50 mM Tris·HCl, pH 8.5, 0.2 mM dithiothreitol, 25 U RNAse inhibitor, and 40 U AMV reverse transcriptase. The mixture was incubated at 30°C for 10 min and 42°C for 1 hr, followed by inactivation of the enzyme at 99°C for 5 min.

7. Real–time quantitative polymerase chain reaction (qPCR)

I compared the transcript levels of mouse and human *ABCA1*, peroxisome proliferator–activated receptor gamma coactivator 1–alpha (*Ppargc1α*), and the genes related to β–oxidation and apoptosis by qPCR. The RNAs used for amplification were 25 ng per reaction tube. Using the ABI PRISM 7700 Sequence Detection System (Applied Biosystems, Foster City, CA, USA), a total volume of 20 μL mixture in each well was used containing 10 μL of SYBR Green PCR Master Mix (Applied Biosystems, Foster City, CA, USA), 5 μL of cDNA, and 5 pmol sense and antisense primers. The sequences of primers are presented in Table 1. The PCR conditions were as follows: 35 cycles of denaturation for 30 min at 94.5°C, annealing for 30 sec at 60°C, and extension for 1 min at 72°C.

Initial heating for 9 min at 95°C and final extension for 7 min at 72°C were performed for all PCR reactions. Each sample was run in triplicate in separate tubes, and a control without cDNA was also run in parallel with each assay. After real–time PCR, the temperature was increased from 60°C to 95°C at a rate of 2°C /min to construct a melting curve. The cDNA content of each specimen was determined using a comparative CT method with 2-$^{\Delta\Delta}$CT.[22] The results are given as the relative expression normalized to the expression of 18s rRNA and expressed in arbitrary units.

Table 1. Sequences of oligonucleotide primers used for qPCR test

Genes		Sequences
Human	**Forward**	ATGGCTTGTTGGCCTCAGC
ABCA1	**Reverse**	AGCAGCAGCTGACATGTTTGT
Mouse	**Forward**	ACATCCTGAAGCCAGTTGTG
Abca1	**Reverse**	CCAAGCTGTCAAGCAACACT
Ppargc1a	**Forward**	AGTCCCATACACAACCGCAG
	Reverse	CCCTTGGGGGTCATTTGGTGA
Cpt1	**Forward**	GGTCTTCTCGGGTCGAAAGC
	Reverse	TCCTCCCACCAGTCACTCAC
Acox1	**Forward**	CTTGGATGGTAGTCCGGAGA
	Reverse	TGGCTTCGAGTGAGGAAGTT
Bcl2	**Forward**	TGGGATGCCTTTGTGGAACT
	Reverse	CAGCCAGGAGAAATCAAACAGA
Bax	**Forward**	TCCACCAAGAAGCTGAGCGAG
	Reverse	GTCCAGCCCATGATGGTTCT
18s	**Forward**	AACTAAGAACGGCCATGCAC
	Reverse	CCTGCGGCTTAATTTGACTC

8. Western blot analyses

Protein expression levels of mouse ABCA1 and apoptosis-related markers were examined with Western blot analyses. Pieces of tissue and harvested cultured cells were lysed in SDS sample buffer [2% SDS, 10 mM Tris·HCl, pH 6.8, 10% (vol/vol) glycerol]. Lysates were centrifuged at $10,000 \times g$ for 10 min at 4°C, and the supernatant was stored at -70°C until use. Protein concentration was determined using the Bio-Rad protein assay kit (Bio-Rad Laboratories, Inc., Hercules, CA, USA). Laemmli sample buffer was added to aliquots of the extracts containing 30 μg of protein and was heated for 5 min at 100°C. Proteins

10

were resolved by electrophoresis on 5–15% acrylamide denaturing SDS–polyacrylamide gels, transferred onto nitrocellulose or polyvinylidene difluoride membranes, and probed with the antibodies against the following proteins: ABCA1 (1:500; ab18180; Abcam, Cambridge, UK), PGC1-α (1:1,000; ab54481; Abcam), BCL2 (1:1,000; sc-509; Santa Cruz Biotechnology, Santa Cruz, CA, USA), BAX (1:1,000; sc-493; Santa Cruz Biotechnology, Santa Cruz, CA, USA), cleaved caspase 3 (1:500; 9661; Cell Signaling Technology), and β-actin (1:10,000; A5316; Sigma Chemical Co., Perth, Australia). The membranes were washed three times for 10 min in 1 × TBS with 0.1% Tween-20 and incubated in buffer A containing a 1:2,000 dilution of horseradish peroxidase–conjugated anti-rabbit (7074; Cell Signaling Technology) or anti-mouse IgG antibody (7076; Cell Signaling Technology) was served as a secondary antibody. After repeated washes, the membrane was developed by chemiluminescence (Western Lightning-ECL; Thermo Scientific). To quantify the band densities, I used ImageJ v1.49 software (National Institutes of Health, Bethesda, MD, USA; online at http://rsbweb.nih.gov/ij).

9. RhoA activity assay

RhoA activity was assessed using the RhoA pull-down assay (BK036; Cytoskeleton, Inc., Denver, CO, USA) following the manufacturer's protocols. GTP-bound RhoA was then immunoprecipitated from cleared lysate with glutathione S-transferase-tagged Rhotekin-Rho-binding domain protein bound to Glutathione Agarose. The beads were washed and the immunoprecipitates were analyzed by Western blot analysis using a RhoA-specific monoclonal antibody.

The lysate (30 μg) was also probed for RhoA to ensure equality across conditions. Expression analysis was performed by Western blotting using a RhoA-specific antibody.

10. Cholesterol and triglyceride assay

4 x 10^6 podocytes and 10 mg kidney cortex tissues for each different group were used for total cholesterol and triglyceride measurement with a cholesterol assay kit (10007640; Cayman Chemical, Ann Arbor, MI, USA) and a triglyceride assay kit (10010303; Cayman Chemical, Ann Arbor, MI, USA). In short, cells or kidney tissues were suspended in 200 ml of chloroform/isopropanol/NP-40 (7:11:0.1) mixture buffer, homogenized, centrifuged at room temperature with x15000g and collected supernatant in the new EP tube. The supernatant was incubated at 50°C until the buffer evaporated, then diluted with assay buffer and measured the kit.

11. Immunofluorescence staining

For double-immunofluorescence staining using mouse kidney samples, 5 μm-thick cryosections were hydrated with acetone for 30 minutes and followed by air dry for 10 min. Sections were blocked in 5% normal donkey serum for 30 minutes at room temperature and incubated overnight at 4°C with a mouse anti-ABCA1 (1:100; ab18180; abcam), active RhoA mouse mAb (1:100; ARH04; Cytoskeleton, Inc., Denver, CO), Acti-stain 670 phalloidin (200nM; PHDN1-A; Cytoskeleton, Inc.) and a rabbit anti-synaptopodin (1:10,000; 163002; Synaptic Systems) overnight at 4°C. Anti-mouse Cy3 (1:200; 4408; Cell Signaling Technology) and anti-rabbit FITC (1:200; 4413; Cell Signaling Technology) were applied at room temperature for 1 hour, and nuclei were stained with DAPI.

12. Bodipy 493/503 staining

For lipid droplets staining, 20 μm-thick cryosections of kidney tissue and stimulated mouse podocytes cultured in the chamber were fixed in 4% paraformaldehyde for 10 min, washed in PBS three times and incubated for 60 min at room temperature with 5ug/ml of fluorescent neutral lipid stain Bodipy 403/503 (D3922; Life Technologies). After washing, the tissue sections and slide

with the podocytes attached were counterstained with DAPI and mounted with Vectashield (Vector Liboratories, Burlingame, CA, USA).

13. Measurement of oxygen consumption rate and extracellular acidification rate

A Seahorse Bioscience XF24 extracellular flux analyzer was used to measure the rate change of dissolved oxygen in medium immediately surrounding adherent cells cultured in an XF24 V7 cell culture microplate (Seahorse Bioscience, North Billerica, MA, USA). Mouse podocyte cells were cultured in RPMI supplement with 1% FBS and seeded in a XF24 V7 cell culture microplate at 1.0×10^4 cells per well. Oxygen consumption rates (pmol/minute) and the extracellular acidification rate (mpH/minute) were assessed at baseline and after the addition of oligomycin (2 μM), the uncoupler FCCP (0.5 μM) and the electron transport inhibitor Rotenone (0.5 μM).

14. Urinary albumin and creatinine measurement

Urine was collected for 24 hours using a metabolic cage, followed by immediate centrifugation at 4°C and gathering of the supernatant. Urinary albumin and creatinine were diluted with a different dilution factor and measured using Albuwell M kit (1011; Exocell, Inc., Philadelphia, PA, USA) according to the manufacturer's instructions.

15. Transmission electron microscopy examination

Podocyte foot effacement, mitochondrial structure and lipid droplets in the kidney tissue were examined by standard transmission electron microscopy (TEM) (JEOL 1011 microscope, Tokyo, Japan). 1×10^6 mouse podocytes and 1×1 mm^3 kidney cortex tissues were fixed with a mixture of 2% paraformaldehyde and 2.5% glutaraldehyde overnight, washed, dehydrated, and embedded in a resin according to standard procedures.

16. Statistical analysis

Statistical analysis was performed using the statistical package SPSS software version 20.0 for Windows (SPSS, Chicago, IL, USA). All the results are presented as mean ± SD. To analyze the difference between two groups, a Student's t-test was used. A one-way ANOVA with a post hoc Bonferroni's test was applied when more than two groups were present. A difference with a P-value < 0.05 was considered statistically significant.

III. RESULTS

1. Glomerular expression of ABCA1 decreases in FSGS animal models

I performed the microarray analysis to identify the signal pathway in FSGS animal models. In GO biological analysis, the DEGs were enriched in the process of fatty acid metabolism, the lipid biosynthesis, and transmembrane transport, etc. (**Fig. 1A**).

The transcript level of glomerular *Abca1* was examined in the tissue samples obtained from the patients with FSGS. The clinical characteristics of the patients are shown in **Table 2**. Glomerular *Abca1* mRNA expression was significantly reduced in patients with FSGS as compared to the control and IgAN groups (**Fig. 1B**).
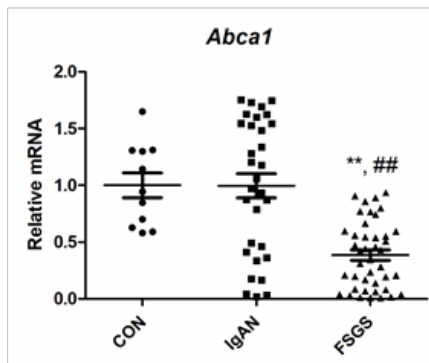
A
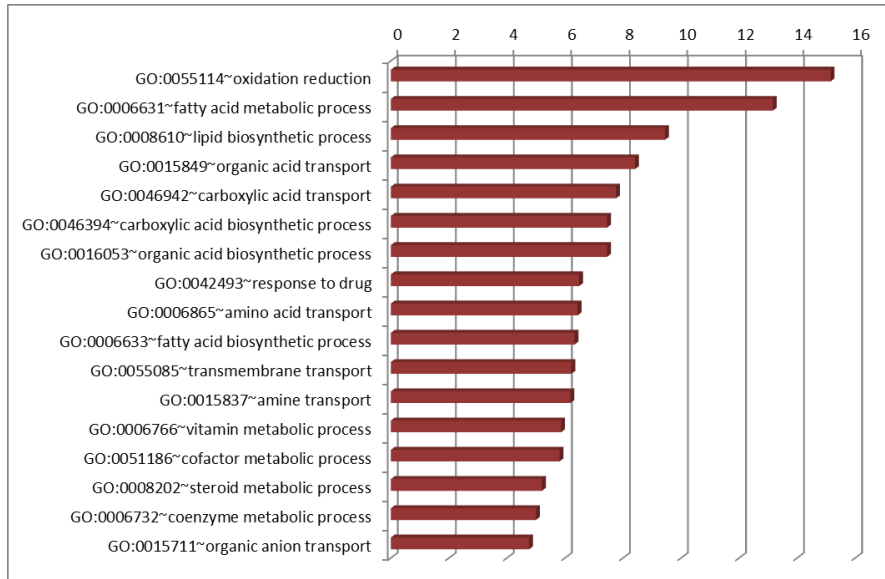
B

Figure 1. Identification of biological pathways of DEGs and decreased ABCA1 expression in FSGS animal models.

(A) Top enriched of GO enrichment analysis of the DEGs in FSGS animal model. **(B)** *Abca1* mRNA expression in glomerular samples from patients with FSGS.

Note: **; $p < 0.001$ vs. CON, ##; $p < 0.001$ vs. IgAN.

CON, control; IgAN, IgA nephropathy; FSGS, focal segmental glomerulosclerosis.

Table 2. Clinical characteristics of patients

| Variables	CON (*n* = 20)	IgAN (*n* = 50)	FSGS (*n* = 43)	*P*
Age (years)	23.8 ± 10.9	39.1 ± 11.7	44.5 ± 16.4	<0.001
Male (*n*, %)	18 (90)	16 (32)	32 (53)	<0.001
BUN (mg/dL)	12.4 ± 2.9	14.9 ± 4.5	22.4 ± 20.4	<0.001
Creatinine (mg/dL)	0.9 ± 0.2	0.9 ± 0.3	1.51 ± 1.51	<0.001
eGFR (mL/min/1.73 m^2)	116 ± 18	91 ± 23	72.0 ± 33.7	<0.001
Cholesterol (mg/dL)	160 ± 33	196 ± 43	243.1 ± 127.7	0.001
Triglyceride (mg/dL)	98 ± 41	146 ± 111	212.5 ± 153.3	0.005
HDL–C (mg/dL)	50 ± 7	54 ± 15	53.0 ± 21.8	0.87
LDL–C (mg/dL)	81 ± 25	118 ± 36	138.2 ± 72.6	0.04
UPCR (g/g Cr)	0.26 ± 0.31	1.79 ± 1.38	4.63 ± 6.78	<0.001
UACR (mg/g Cr)	201 ± 277	1374 ± 1060	3158.5 ± 4489.5	<0.001

IgAN, IgA nephropathy; FSGS, focal segmental glomerulosclerosis; BUN, blood urea nitrogen; eGFR, estimated glomerular filtration rate; HDL–C, high–density lipoprotein cholesterol; LDL–C, low–density lipoprotein cholesterol; UPCR, urine protein to creatinine ratio; UACR, urine albumin to creatinine ratio.

2. Podocyte-specific deletion of ABCA1 has increased in podocyte injury and lipid accumulation in FSGS animal models

Reduced expression of ABCA1 was confirmed by double immunofluorescence staining in the podocyte of the FSGS models. A significant decrease in ABCA1 expressions was observed in the ADR group compared to those of the control group. Furthermore, ABCA1 in podocytes showed dramatic decreases in podocyte-specific *Abca1* knock out mice (**Fig. 2A**).

Regarding the electron microscopy findings, foot processes were effaced in FSGS models and these abnormalities were much more prominent in podocyte-specific *Abca1* KO ADR mice (**Fig. 2B**). Furthermore, the albuminuria was significantly increased in the FSGS group, which was much higher in the podocyte-specific *Abca1* KO ADR group compared to that of the WT ADR group (**Fig. 2C**). In Bodipy staining, FSGS mice were characterized by an increased glomerular lipid accumulation when compared with WT mice (**Fig. 2D**). Glomerular lipid accumulation was much higher in podocyte-specific *Abca1* KO ADR models compared to that in WT ADR groups. The levels of total cholesterol and triglycerides in the kidney tissues were significantly higher in WT FSGS groups than in the WT groups, but the highest lipid levels were observed in podocyte-specific *Abca1* KO ADR groups (**Fig. 2E**).
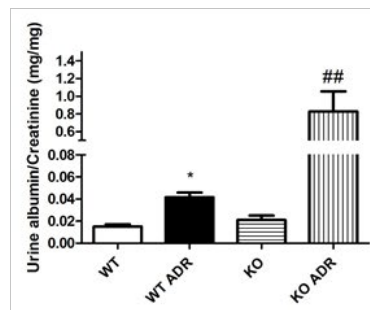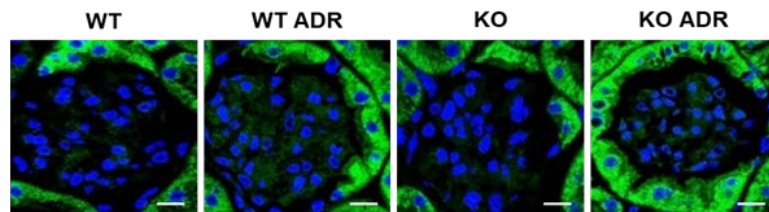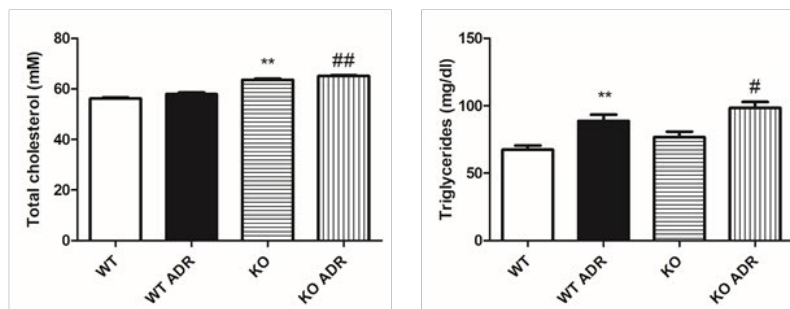
A
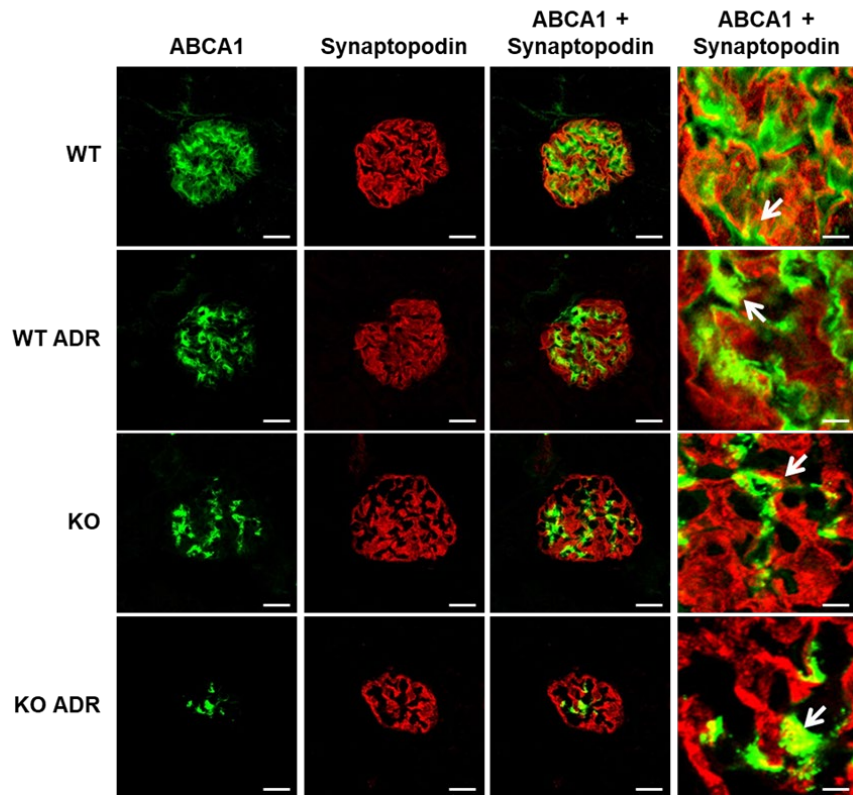
B
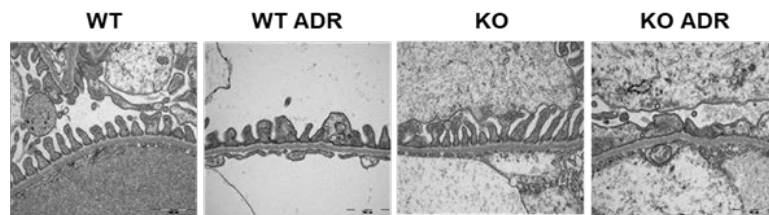
C

D

E

Figure 2. Podocyte-specific deletion of ABCA1 has increased in podocyte injury and lipid accumulation in FSGS models.

(A) Representative image of double IF staining of ABCA1 and synaptopodin in

WT, WT ADR, KO, and KO ADR mice. **(B)** Representative transmission electron microscopy images of podocyte foot process measurements in animal models. **(C)** UACR for mice from different experimental groups. **(D)** Bodipy staining of glomerular cholesterol accumulation in animal models. **(E)** Total cholesterol and triglyceride levels in the kidneys from animal models.

Note: *; $p < 0.05$ vs. WT, #; $p < 0.05$ vs. WT ADR, **; $p < 0.001$ vs. WT, ##; $p < 0.001$ vs. WT ADR.
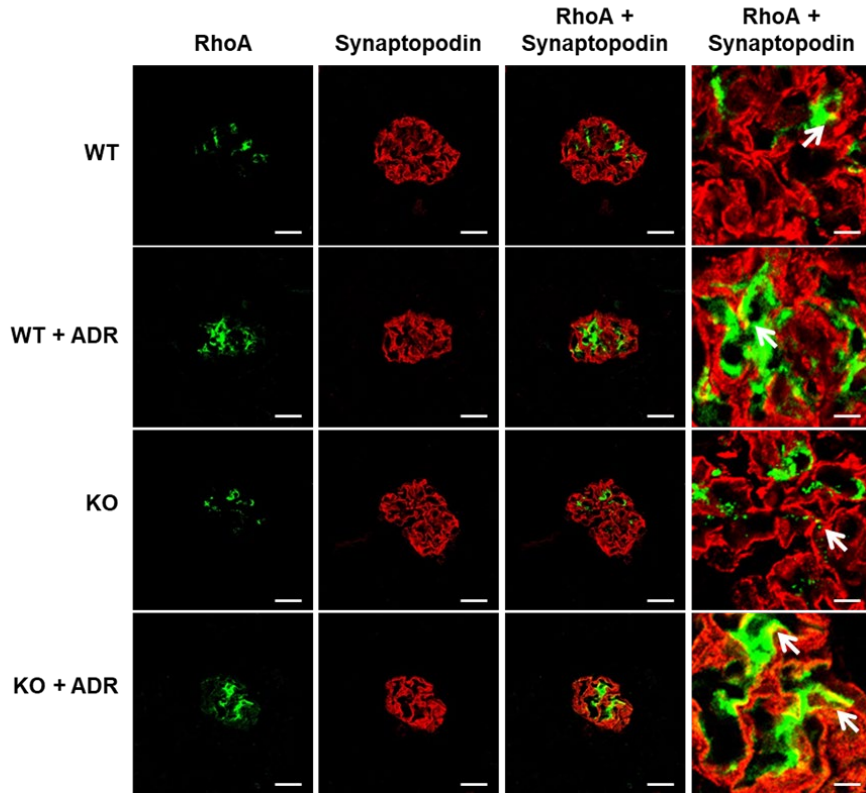
WT, wild type; ADR, Adriamycin; KO, knockout; UACR, urine albumin to creatinine ratio; IF, immunofluorescence.

3. ABCA1 deficiency leads to the alteration of RhoA activity, mitochondrial fatty acid oxidation and mitochondrial morphology in FSGS animal models

In a previous study it was shown that, abnormal RhoA activity was found to be involved in podocyte injury leading to FSGS.[23] Using immunofluorescence staining, I confirmed that active RhoA was significantly increased in the podocyte of WT ADR groups. Moreover, I found a more prominent increase in active RhoA staining in the podocyte-specific *Abca1* KO ADR groups than in the WT ADR groups (**Fig. 3A**).

I examined mitochondrial fatty acid oxidation and apoptosis-related mRNA and protein expressions in FSGS models. Transcript and protein expression levels of PGC-1α, a key regulator of mitochondrial biogenesis, were significantly decreased in the WT ADR groups. In fatty acid oxidation markers, transcript levels of *Cpt1* and *Acox1* were significantly increased in WT ADR mice, which were much higher in podocyte-specific *Abca1* KO ADR mice. In apoptosis markers, compared to wild type ADR mice, the expression of Bcl2 was significantly decreased, whereas the expressions of Bax and Cleaved-caspase3 were significantly increased in podocyte-specific *Abca1* KO ADR groups (**Fig. 3B-D**). Transmission electron microscopy showed that mitochondria were prominently swelled and the cristae were destroyed in the podocyte of podocyte-specific *Abca1* KO ADR mice (**Fig. 3E**).
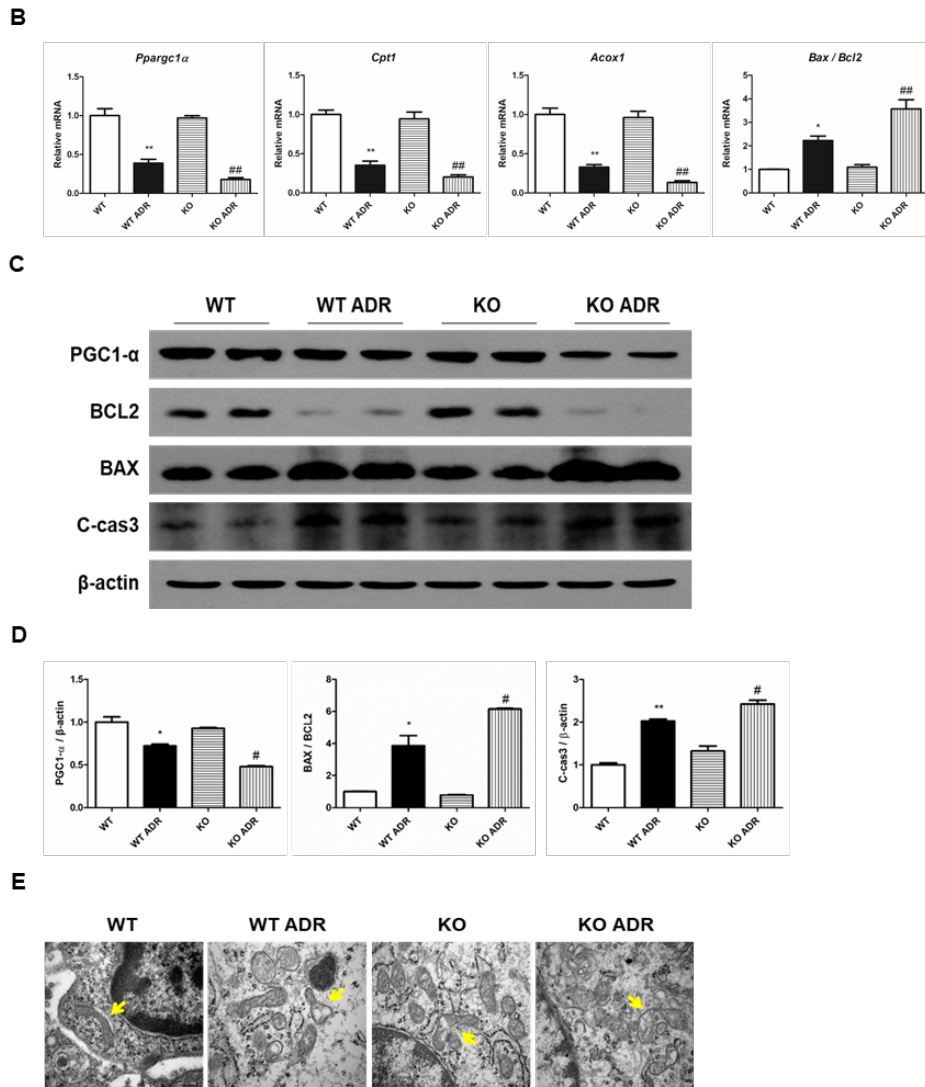
A

Figure 3. ABCA1 deficiency leads to the alteration of RhoA activity, mitochondrial morphology and fatty acid oxidation in FSGS animal models. **(A)** Double IF staining of RhoA and synaptopodin in WT, WT ADR, KO, and KO ADR mice. **(B)** The transcription levels of *Ppargc1a*, *Cpt1*, *Acox1*, *Bcl2* and *Bax* in animal models. **(C and D)** Western blot analysis of PGC1-α, BCL2, BAX and C-cas3 in KO ADR models. **(E)** Transmission electron microscopy images of mitochondria (mitochondria are marked with yellow asterisks).
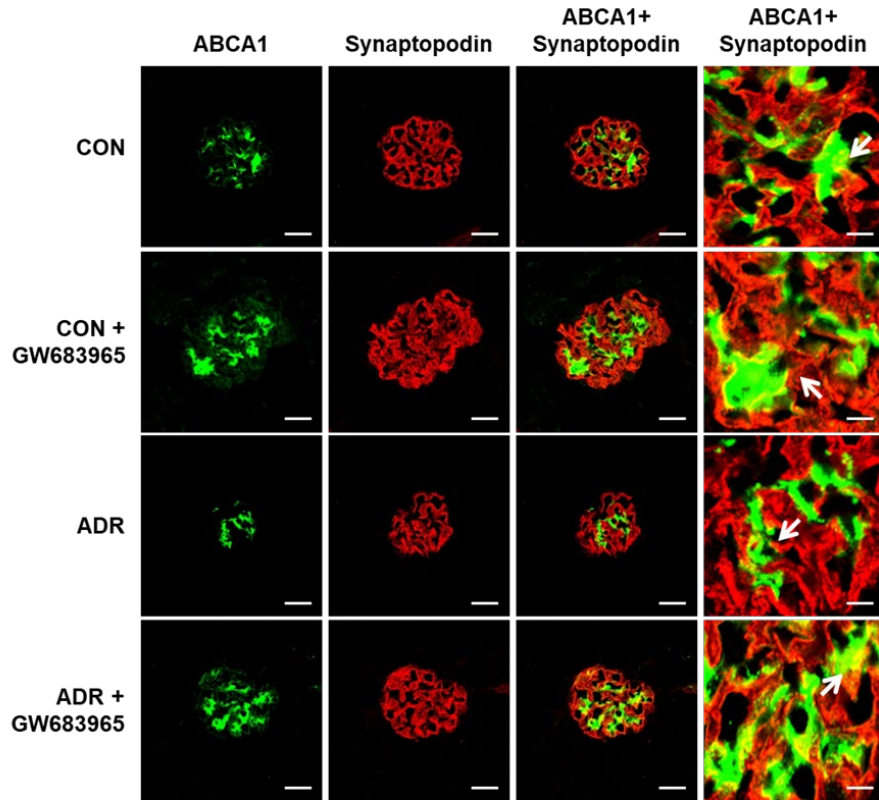
24

Note: *; $p < 0.05$ vs. WT, #; $p < 0.05$ vs. WT ADR, **; $p < 0.001$ vs. WT, ##; $p < 0.001$ vs. WT ADR.

WT, wild type; ADR, Adriamycin; KO, knockout; PGC–1α, peroxisome proliferator–activated receptor gamma coactivator 1–alpha; Cpt1, carnitine palmitoyltransferase–1; Acox1, acyl–CoA oxidase; IF, immunofluorescence.
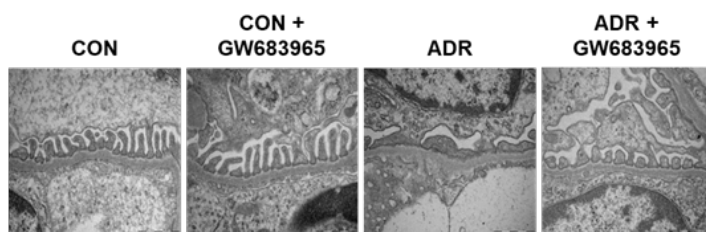
4. Restoration of the podocyte injury and lipid accumulation by LXR agonist via ABCA1 overexpression in FSGS animal models

I tried to upregulate ABCA1 expression with LXR agonist (GW683965) treatment. Liver X receptor alpha (LXRα), which is upstream of ABCA1, activated a transcriptional cascade to modulate the expression of ABCA1 and increase in cholesterol efflux.[24] ABCA1 expression was restored by LXR treatment in ADR-treated BALB/C mice (**Fig. 4A**). As expected, GW683965 improved foot process effacement and significantly reduced in albuminuria (**Fig. 4B and C**). Also, Bodipy 493/503 staining showed that glomerular lipid accumulation was improved after treatment of GW683965 in FSGS mice. The cholesterol and triglyceride levels in the kidney were also reduced in FSGS models treated by GW683965 (**Fig. 4E**).
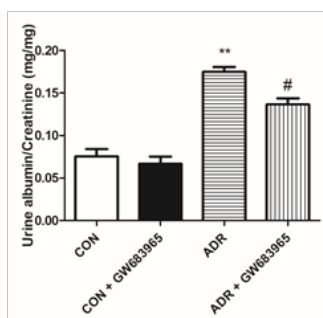
A

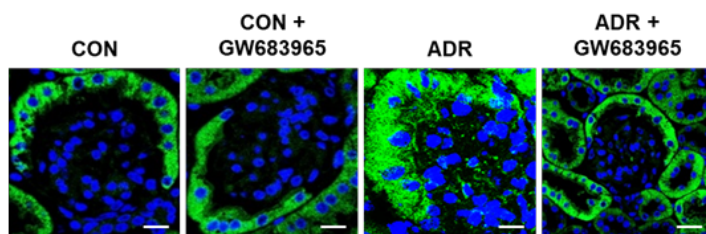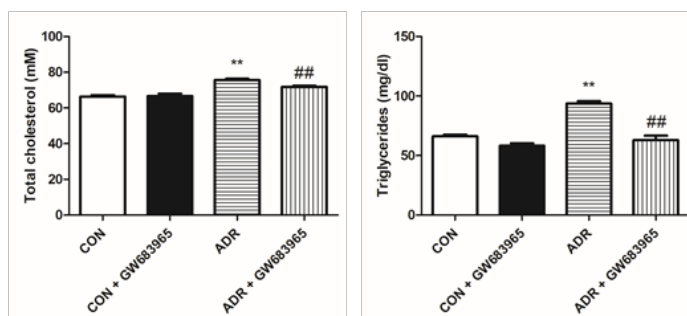|	ABCA1	Synaptopodin	ABCA1+ Synaptopodin	ABCA1+ Synaptopodin
CON				
CON + GW683965				
ADR				
ADR + GW683965				

Figure 4. Restoration of the podocyte injury and lipid accumulation by ABCA1 overexpression in ADR-treated BALB/C mice.

(A) Double IF staining of ABCA1 and synaptopodin in ADR (CON, CON + GW683965, ADR, ADR + 683965) groups. **(B)** TEM images of podocyte in animal models. **(C)** UACR in animal models. **(D)** Bodipy staining of intraglomerular cholesterol accumulation in animal models. **(E)** Total cholesterol and triglyceride levels in the kidneys from animal models.

Note: **; $p < 0.001$ vs. CON, #; $p < 0.05$ vs. ADR, ##; $p < 0.001$ vs. ADR.

WT, wild type; ADR, Adriamycin; UACR, urine albumin to creatinine ratio; IF, immunofluorescence

5. LXR agonist attenuates the RhoA activity, mitochondrial morphology and fatty acid oxidation in FSGS animal models

RhoA activity increased in ADR-treated BALB/C mice, however, GW683965 reduced the staining of active RhoA in these animals **(Fig. 5A)**. Compared to the control, the expression of PGC1-α was significantly decreased in the ADR groups. Also, the transcript levels of fatty acid oxidation-related markers were significantly decreased in the ADR groups. These reduced expressions significantly went up by GW683965 **(Fig. 5B-D)**. Abnormal mitochondrial morphology from ADR groups assessed by TEM was also alleviated by GW683965 **(Fig. 5E)**.

A

B

C

D

E
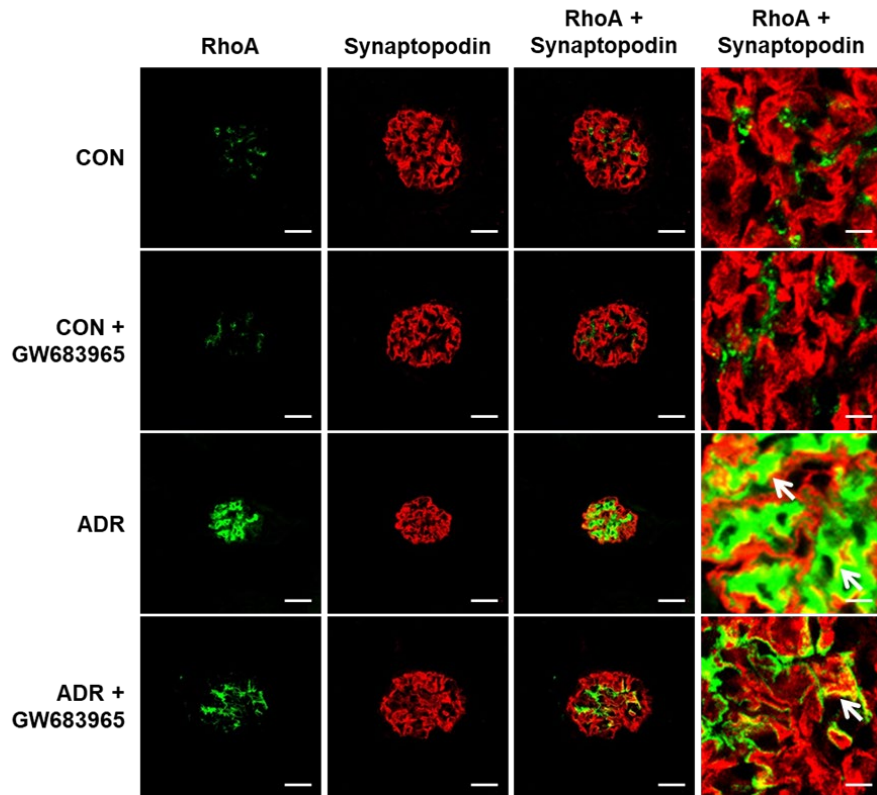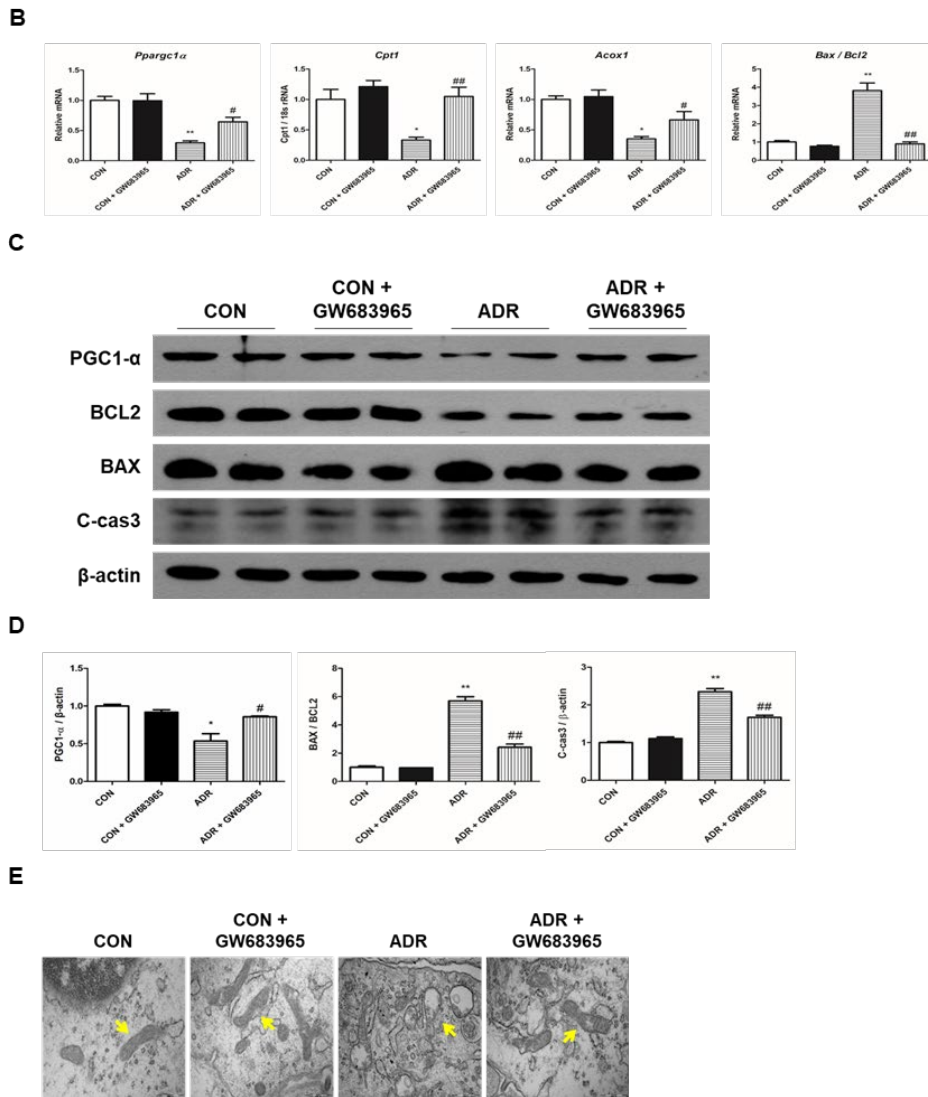
Figure 5. LXR agonist attenuates alteration of RhoA activity, mitochondrial morphology and fatty acid oxidation in ADR-treated BALB/C mice.

(A) Double IF staining of RhoA and synaptopodin in GW683965-treated ADR (CON, CON + GW683965, ADR, ADR + 683965) groups. **(B)** The transcription levels of *Ppargc1a*, *Cpt1*, *Acox1*, *Bcl2* and *Bax* in ADR models. **(C and D)** Western blot analysis of PGC1-α, BCL2, BAX and C-cas3 in the ADR models.

32

(E) TEM images of mitochondria in the glomerulus of the ADR models (mitochondria marked with yellow asterisks).

**Note:** *; $p < 0.05$ vs. CON, #; $p < 0.05$ vs. ADR, **; $p < 0.001$ vs. CON, ##; $p < 0.001$ vs. ADR.

WT, wild type; ADR, Adriamycin; PGC–1α, peroxisome proliferator–activated receptor gamma coactivator 1–alpha; Cpt1, carnitine palmitoyltransferase–1; Acox1, acyl–CoA oxidase; IF, immunofluorescence; TEM, transmission electron microscopy.

## 6. LXR agonist upregulates ABCA1 and recovers podocyte damages in ADR-and TNF-α-stimulated podocytes

In vitro, the transcript and protein expression of ABCA1 were reduced in podocytes stimulated with ADR and TNF-α and it was significantly recovered when treated with GW683965 **(Fig. 6A-C)**. In podocytes stimulated with ADR, and TNF-α, intracellular cholesterol was significantly increased, but it was significantly restored by GW683965 **(Fig. 6D and E)**.

In terms of mitochondrial energy metabolisms, compared to controls, the expression of PGC1-α was significantly decreased in ADR and TNF-α-treated podocytes. These abnormalities were significantly ameliorated by GW683965. And the expression levels of fatty acid oxidation-related markers and apoptosis-related markers were significantly decreased in ADR and TNF-α -treated cells, which were notably restored by GW683965 **(Fig. 7A-C)**. There were significant defects in mitochondrial morphology, evidenced by disrupted cristae and fragmented mitochondria in ADR and TNF-α -treated podocytes. Increased expression of ABCA1 through GW683965 partially recovered mitochondrial morphologic deformities **(Fig. 7D)**. Mitochondrial respiration examined by seahorse analysis was suppressed with ADR and TNF-α stimulated and GW683965 treatment improved the mitochondrial respiration, suggesting that the mitochondria function was restored **(Fig. 7E)**.
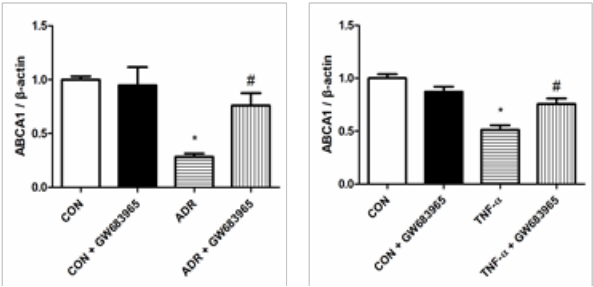
A

B

C

D

CON | CON + GW683965 | ADR | ADR + GW683965 | TNF-α | TNF-α + GW683965
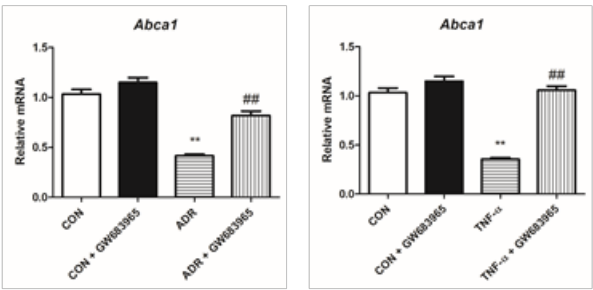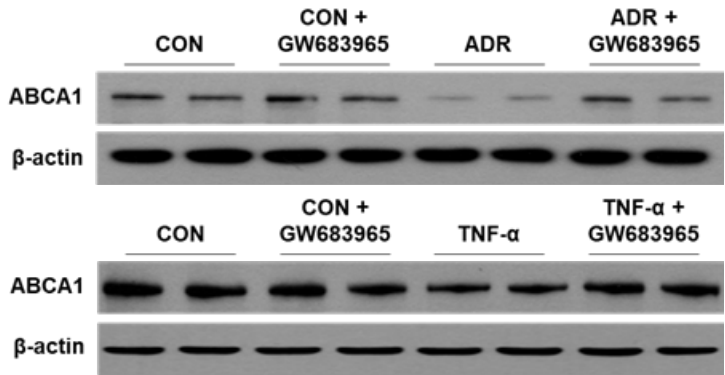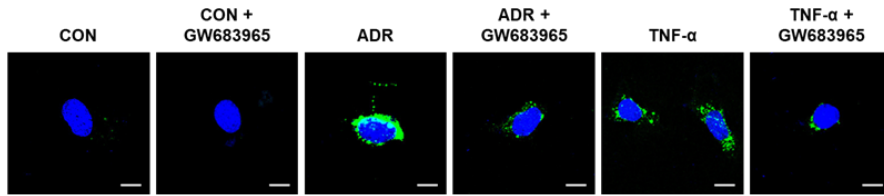
E
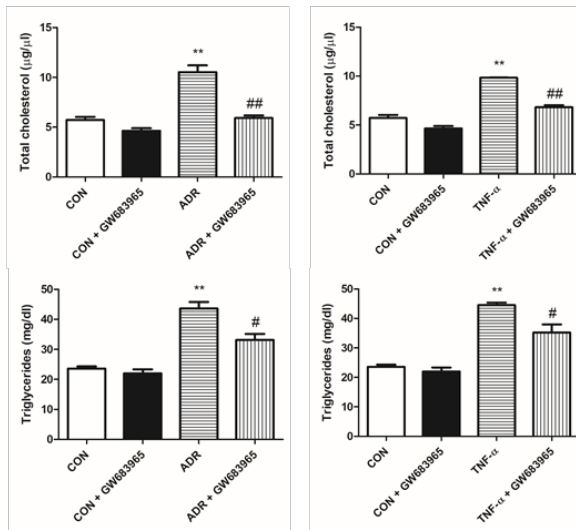
Figure 6. Decreased ABCA1 has increased lipid accumulation in ADR-and TNF-α-stimulated podocytes.

(A) The transcription levels of Abca1 in CON, CON + GW683965, ADR or TNF-α, ADR + GW683965 or TNF-α + GW683965. **(B and C)** Western blot analysis of ABCA1 in ADR, TNF-α stimulated podocytes. **(D)** Staining of Bodipy in ADR- and TNF-α-induced podocytes. **(E)** Total cholesterol and triglyceride levels in ADR, TNF-α stimulated podocytes.

Note: *; $p < 0.05$ vs. CON, #; $p < 0.05$ vs. ADR or TNF- α, **; $p < 0.001$ vs. CON, ##; $p < 0.001$ vs. ADR or TNF-α.

CON, control; ADR, Adriamycin.

A

B

C

37
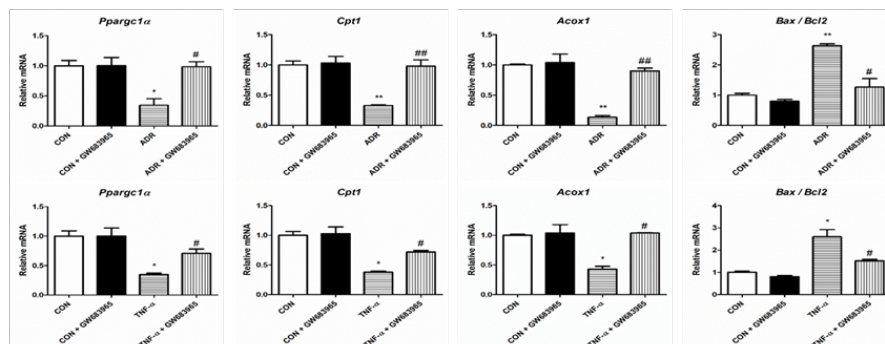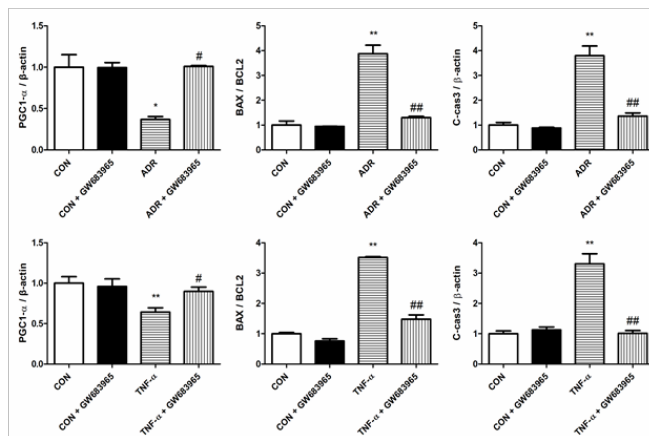
D
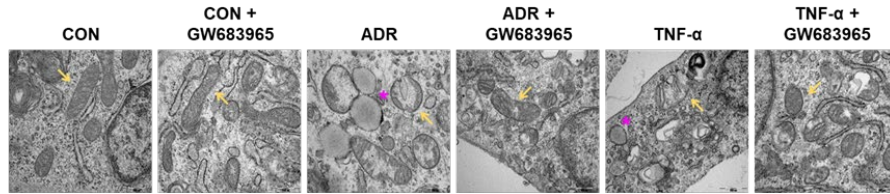
E
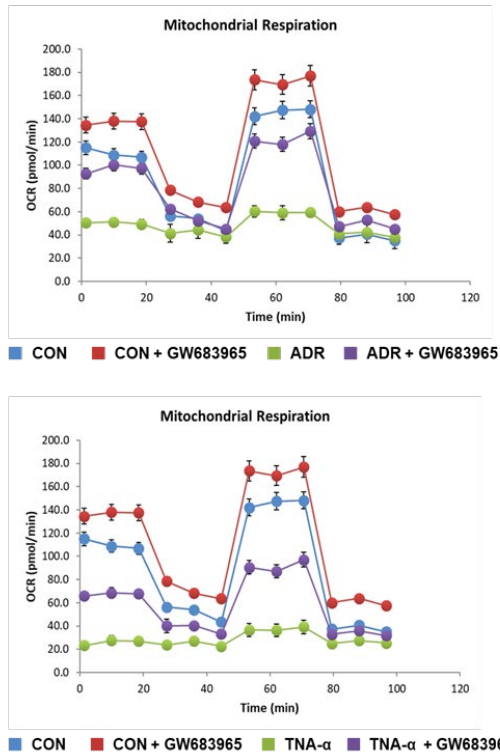
Figure 7. Restoration of mitochondrial morphology and fatty acid oxidation by ABCA1 overexpression in ADR-and TNF-α-stimulated podocytes.

(A) The transcription levels of *Ppargc1α*, fatty acid oxidation, apoptosis-related markers in CON, CON + GW683965, ADR or TNF-α, ADR + GW683965 or TNF-α + GW683965. **(B and C)** Western blot analysis revealed that the protein expression of PGC1-α and apoptosis markers in ADR, TNF-α stimulated podocytes. **(D)** Transmission electron microscopy images of mitochondria in ADR- and TNF-α-induced podocytes. **(E)** The seahorse analysis in ADR, TNF-α
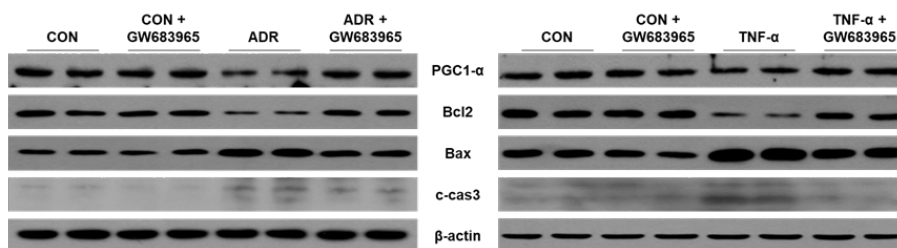
stimulated podocytes.

Note: *; $p < 0.05$ vs. CON, #; $p < 0.05$ vs. ADR or TNF- α, **; $p < 0.001$ vs. CON, ##; $p < 0.001$ vs. ADR or TNF- α.

CON, control; ADR, Adriamycin; PGC–1α, peroxisome proliferator–activated receptor gamma coactivator 1–alpha; Cpt1, carnitine palmitoyltransferase–1; Acox1, acyl–CoA oxidase; OCR, oxygen consumption rate; TEM, transmission electron microscopy.

7. LXR agonist attenuates the RhoA activation in ADR- and TNF-α-stimulated podocytes

ADR and TNF-α-induced podocytes increased in GTP-RhoA (active form). Enhanced RhoA activity by various stimuli was suppressed by GW683965 treatment in podocytes, which is demonstrated in the semiquantitative analysis displayed **(Fig. 8A and B)**. Cytoskeletal remodeling was assessed using confocal laser microscopy. Actin stress fiber in cultured podocytes was disturbed by ADR and TNF-α. However, ADR and TNF-α induced actin stress fiber distortion was dramatically recovered in the podocytes co-treated with GW683965 **(Fig. 8C)**.

A
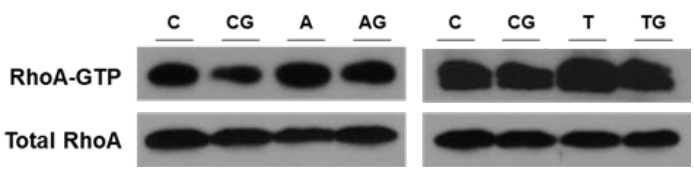
B
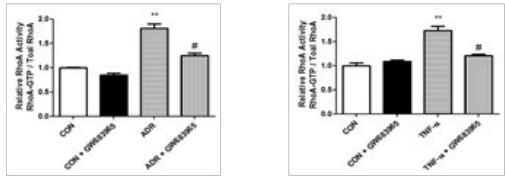
C
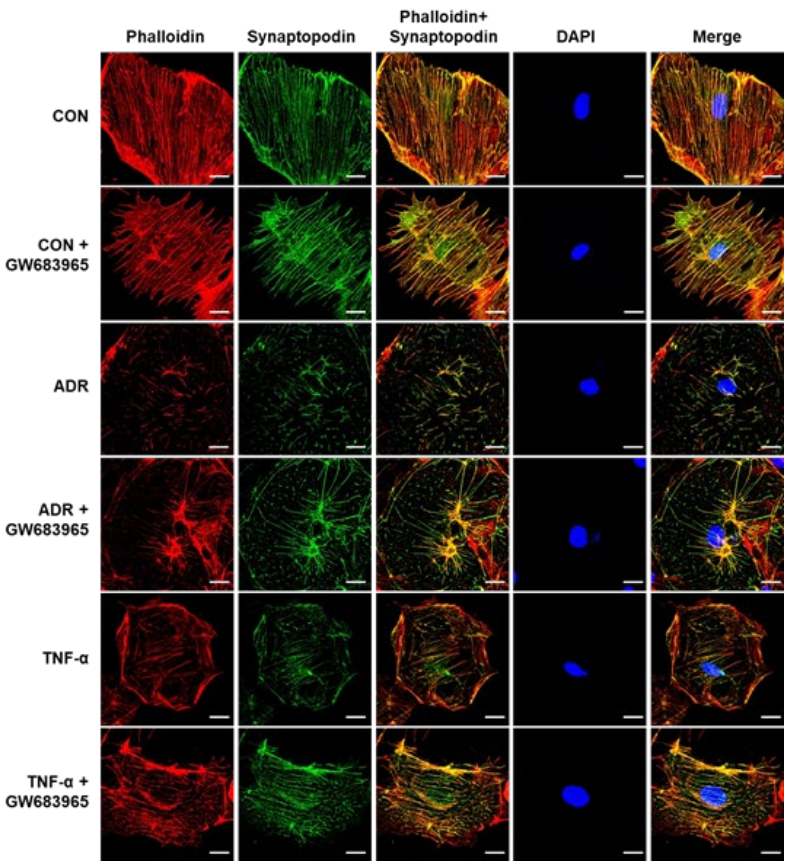
Figure 8. LXR agonist blocks RhoA protein activation in ADR-and TNF-α-stimulated podocytes.

(A and B) RhoA activity in CON, CON + GW683965, ADR or TNF-α, ADR + GW683965 or TNF-α + GW683965 podocyte cells was evaluated by a RhoA pull-down assay. **(C)** Confocal microscopy on actin cytoskeletal remodeling in ADR- and TNF-α-induced podocyte cells.

Note: *; $p < 0.05$ vs. CON, #; $p < 0.05$ vs. ADR or TNF- α, **; $p < 0.001$ vs. CON.

CON, control; CG, control + GW683965; A or ADR, Adriamycin; T, TNF-α; AG, Adriamycin + GW683965; TG, TNF-α + GW683965; IF, immunofluorescence.

IV. DISCUSSION

In this study, I evaluated the role of ABCA1 in the podocyte injury and proteinuria in FSGS. The expression of ABCA1 was significantly decreased and reduced ABCA1 was associated with intracellular lipid accumulation and RhoA activation in experimental FSGS models. These abnormalities resulted in the impairment of mitochondrial function, and finally led to podocyte apoptosis. These abnormalities were significantly recovered by LXR-α treatment via up-regulation of ABCA1 in experimental FSGS models.

ABCA1 is a transmembrane protein which, in an ATP-dependent mechanism, regulates the efflux of cholesterol and phospholipids, and participates in the cellular lipid homeostasis.[25] Previous studies reported that ABCA1 is negatively correlated with the severity of glomerulosclerosis, and ABCA1 is directly correlated with the podocyte number,[10,26] but the exact pathologic mechanisms for podocytopathy have not been thoroughly examined. To examine the role of ABCA1 on the development of FSGS, firstly, we screened the microarray analysis and identified lower *Abca1* mRNA expression in ADR-induced FSGS mice compared to that in the control. In addition, the glomerular transcriptional levels of ABCA1 in patients with FSGS were significantly lower than in those of healthy controls and patients with IgA nephropathy. I also observed the same trend of ABCA1 level in ADR-induced FSGS mouse models. In the animal model of FSGS, after 4–6 weeks of administration of 10.5 mg/kg of ADR to BALB/C mice, an increase in proteinuria and glomerular changes were observed. However, it is known that ADR in C57BL/6 mice do not cause significant FSGS and proteinuria.[27] Meanwhile, FSGS phenotype was observed in ADR treated podocyte specific *Abca1* KO C57BL/6 mice.

Since ABCA1 has a biological function to transport the intracellular cholesterol to extracellular space, reduced ABCA1 levels are associated with cholesterol accumulation in glomeruli of the experimental FSGS model. Glomerular lipid

contents including the cholesterol and triglyceride were much higher in the podocyte-specific *Abca1* knockout FSGS animal compared to those in the wild type FSGS mice. Albuminuria was also aggravated in podocyte-specific *Abca1* knockout FSGS animal; however, the LXR agonist reduced the ADR-induced albuminuria through the restoration of ABCA1. These results suggest that ABCA1 is involved in podocyte injury, which is accompanied by lipid accumulation in FSGS.

Lipid accumulation exerts its cytotoxicity via various pathways. Among them, the excessive lipid load can induce the mitochondrial dysfunction and destroy the structure of the mitochondria. The expression of key enzymes related to lipid oxidative metabolism, such as PGC-1α and CPT-1, was significantly reduced in the kidney tissues of patients with diabetic kidney disease (DKD) and DKD animal models (Akita and OVE26 mice). In these animals, the number and size of the lipid droplets were coincidently increased.[28,29] It has also been demonstrated that excessive lipid accumulation in podocytes causes in-cellular lipotoxicity, mitochondrial disfunction and oxidative stress.[30] I also observed dramatic lipid accumulation in the glomeruli and podocytes of the FSGS model, which was accompanied by mitochondrial swelling and the partial or complete disappearance of mitochondrial cristae. Components of the mitochondrial energy metabolism such as PGC-1α, CPT-1 and Acox1 showed lower in the FSGS model.

These changes in mitochondrial function and energy metabolism markers were prominently exacerbated in podocyte-specific *Abca1* knockout FSGS mice and were dramatically reversed by LXR treatment through the recovery of ABCA1 levels. These results indicate that the reduction of ABCA1 in FSGS is involved in the abnormal lipid deposition in podocytes, as well as the damage of mitochondrial function and deterioration of the mitochondrial structure. My study showed that the FSGS model is successfully reproduced in podocyte-specific *Abca1* knockout C57BL/6 mice treated with ADR. This result suggests that lipid

accumulation by down-regulation of ABCA1 might be an important pathophysiologic mechanism for the development of FSGS.

Bax and Bcl2 are the most important pro- and anti-apoptotic proteins, respectively. Their proportion is the key factor in apoptotic regulation. The upregulation of the Bax/Bcl2 ratio increases in the permeability of the mitochondrial membrane, releases pro-apoptotic factors, and then induces or accelerates cellular apoptosis. *In vivo* and *in vitro*, I found that the Bax/Bcl2 ratio and Cleaved caspase3 as an apoptotic marker expression in FSGS renal tissues and podocytes were increased.

The podocyte apoptosis was attenuated when the reduced expression of ABCA1 was reversed by LXR agonist, while the apoptosis-related molecules were dramatically increased after podocyte-specific knocking out in ABCA1. These experimental results show that the reduction of ABCA1 in podocyte and renal tissues of FSGS upregulates the apoptosis in podocytes and ABCA1 agonist reduces the apoptotic signaling pathway.

Interestingly, I observed an increase in RhoA activity in glomeruli of FSGS mice and TNF-α or ADR-treated podocytes. RhoA is a member of the small GTPase family, together with Rac1 and Cdc42.[31] Previous investigations established that too much or too little RhoA activity is equally detrimental to the podocyte. RhoA plays a role in the stabilization of stress fiber in the podocytes; concurrently, increased RhoA activity also results in enhanced apoptosis in the podocytes in DKD. Based on the previous reports, abnormal RhoA activity causes proteinuric kidney disease.[32,33] *In vitro*, TNF-a and ADR treatment enhance the RhoA activity in cultured podocytes, and it was associated with the significant decrease in actin-cytoskeleton stress fiber. The loss of stress fiber was mitigated by the recovery of ABCA1 by the LXR agonist. These results strongly suggest that RhoA is involved in the pathophysiology of lipotoxicity of the podocyte via reduced ABCA1 levels in the podocyte of FSGS. A previous study reported that ROS is involved in RhoA activation.[34] I surmised that RhoA activation might have come from the reduction

in ABCA1 expression in podocytes, which increased intracellular lipid accumulation, and excessive intracellular lipids produced ROS and further induced RhoA activation. This analysis needs to be confirmed by more in-depth research.

V. CONCLUSION

In conclusion, I verified that reduced ABCA1 is involved in the pathophysiology of lipid accumulation and cellular injury in the podocytes under FSGS conditions. The podocyte-specific knockout of *Abca1* aggravated the abnormal lipid deposition in podocytes, further inducing the damage to the mitochondrial structure and function, activated RhoA, and finally resulted in podocyte apoptosis. It is indicated that reversing the ABCA1 is a promising strategy to delay the podocytes' injury of FSGS.

REFERENCES

1. Kitiyakara C, Kopp JB, Eggers P. Trends in the epidemiology of focal segmental glomerulosclerosis. Semin Nephrol 2003;23:172-82.

2. D'Agati VD, Kaskel FJ, Falk RJ. Focal segmental glomerulosclerosis. N Engl J Med 2011;365:2398-411.

3. Naito T, Ercan B, Krshnan L, Triebl A, Koh DHZ, Wei FY, et al. Movement of accessible plasma membrane cholesterol by the GRAMD1 lipid transfer protein complex. Elife 2019;8.

4. Argmann CA, Edwards JY, Sawyez CG, O'Neil CH, Hegele RA, Pickering JG, et al. Regulation of macrophage cholesterol efflux through hydroxymethylglutaryl-CoA reductase inhibition: a role for RhoA in ABCA1-mediated cholesterol efflux. J Biol Chem 2005;280:22212-21.

5. DeBose-Boyd RA. Feedback regulation of cholesterol synthesis: sterol-accelerated ubiquitination and degradation of HMG CoA reductase. Cell Res 2008;18:609-21.

6. Brown MS, Goldstein JL. How LDL receptors influence cholesterol and atherosclerosis. Sci Am 1984;251:58-66.

7. Wang N, Lan D, Chen W, Matsuura F, Tall AR. ATP-binding cassette transporters G1 and G4 mediate cellular cholesterol efflux to high-density lipoproteins. Proc Natl Acad Sci U S A 2004;101:9774-9.

8. Attie AD. ABCA1: at the nexus of cholesterol, HDL and atherosclerosis. Trends Biochem Sci 2007;32:172-9.

9. Tabas I. Consequences of cellular cholesterol accumulation: basic concepts and physiological implications. J Clin Invest 2002;110:905-11.

10. Merscher-Gomez S, Guzman J, Pedigo CE, Lehto M, Aguillon-Prada R, Mendez A, et al. Cyclodextrin protects podocytes in diabetic kidney disease. Diabetes 2013;62:3817-27.

11. Saltiel AR, Kahn CR. Insulin signalling and the regulation of glucose and

lipid metabolism. Nature 2001;414:799-806.

12. Tufro A. Cholesterol accumulation in podocytes: a potential novel targetable pathway in diabetic nephropathy. Diabetes 2013;62:3661-2.

13. Khera AV, Cuchel M, de la Llera-Moya M, Rodrigues A, Burke MF, Jafri K, et al. Cholesterol efflux capacity, high-density lipoprotein function, and atherosclerosis. N Engl J Med 2011;364:127-35.

14. Mitrofanova A, Molina J, Varona Santos J, Guzman J, Morales XA, Ducasa GM, et al. Hydroxypropyl-beta-cyclodextrin protects from kidney disease in experimental Alport syndrome and focal segmental glomerulosclerosis. Kidney Int 2018;94:1151-9.

15. Pedigo CE, Ducasa GM, Leclercq F, Sloan A, Mitrofanova A, Hashmi T, et al. Local TNF causes NFATc1-dependent cholesterol-mediated podocyte injury. J Clin Invest 2016;126:3336-50.

16. Cohen CD, Frach K, Schlondorff D, Kretzler M. Quantitative gene expression analysis in renal biopsies: a novel protocol for a high-throughput multicenter application. Kidney Int 2002;61:133-40.

17. Berthier CC, Zhang H, Schin M, Henger A, Nelson RG, Yee B, et al. Enhanced expression of Janus kinase-signal transducer and activator of transcription pathway members in human diabetic nephropathy. Diabetes 2009;58:469-77.

18. Merscher-Gomez S, Guzman J, Pedigo CE, Lehto M, Aguillon-Prada R, Mendez A, et al. Cyclodextrin protects podocytes in diabetic kidney disease. Diabetes 2013;62:3817-27.

19. Mundel P, Reiser J, Zuniga Mejia Borja A, Pavenstadt H, Davidson GR, Kriz W, et al. Rearrangements of the cytoskeleton and cell contacts induce process formation during differentiation of conditionally immortalized mouse podocyte cell lines. Exp Cell Res 1997;236:248-58.

20. Kang SW, Adler SG, Lapage J, Natarajan R. p38 MAPK and MAPK kinase 3/6 mRNA and activities are increased in early diabetic glomeruli.

Kidney Int 2001;60:543-52.

21. Ge SX, Son EW, Yao R. iDEP: an integrated web application for differential expression and pathway analysis of RNA-Seq data. BMC Bioinformatics 2018;19:534.

22. Rao X, Huang X, Zhou Z, Lin X. An improvement of the 2^(-delta delta CT) method for quantitative real-time polymerase chain reaction data analysis. Biostat Bioinforma Biomath 2013;3:71-85.

23. Yoo TH, Pedigo CE, Guzman J, Correa-Medina M, Wei C, Villarreal R, et al. Sphingomyelinase-like phosphodiesterase 3b expression levels determine podocyte injury phenotypes in glomerular disease. J Am Soc Nephrol 2015;26:133-47.

24. Nakaya K, Tohyama J, Naik SU, Tanigawa H, MacPhee C, Billheimer JT, et al. Peroxisome proliferator-activated receptor-alpha activation promotes macrophage reverse cholesterol transport through a liver X receptor-dependent pathway. Arterioscler Thromb Vasc Biol 2011;31:1276-82.

25. Wang N, Silver DL, Thiele C, Tall AR. ATP-binding cassette transporter A1 (ABCA1) functions as a cholesterol efflux regulatory protein. J Biol Chem 2001;276:23742-7.

26. Herman-Edelstein M, Scherzer P, Tobar A, Levi M, Gafter U. Altered renal lipid metabolism and renal lipid accumulation in human diabetic nephropathy. J Lipid Res 2014;55:561-72.

27. Mayhew E, Rustum Y, Vail WJ. Inhibition of liver metastases of M 5076 tumor by liposome-entrapped adriamycin. Cancer Drug Deliv 1983;1:43-58.

28. Szeto HH, Liu S, Soong Y, Alam N, Prusky GT, Seshan SV. Protection of mitochondria prevents high-fat diet-induced glomerulopathy and proximal tubular injury. Kidney Int 2016;90:997-1011.

29. Weinberg JM. Lipotoxicity. Kidney Int 2006;70:1560-6.

30. Opazo-Rios L, Mas S, Marin-Royo G, Mezzano S, Gomez-Guerrero C, Moreno JA, et al. Lipotoxicity and Diabetic Nephropathy: Novel Mechanistic Insights and Therapeutic Opportunities. Int J Mol Sci 2020;21.

31. Asanuma K, Yanagida-Asanuma E, Faul C, Tomino Y, Kim K, Mundel P. Synaptopodin orchestrates actin organization and cell motility via regulation of RhoA signalling. Nat Cell Biol 2006;8:485-91.

32. Wang L, Ellis MJ, Gomez JA, Eisner W, Fennell W, Howell DN, et al. Mechanisms of the proteinuria induced by Rho GTPases. Kidney Int 2012;81:1075-85.

33. Zhu L, Jiang R, Aoudjit L, Jones N, Takano T. Activation of RhoA in podocytes induces focal segmental glomerulosclerosis. J Am Soc Nephrol 2011;22:1621-30.

34. Aghajanian A, Wittchen ES, Campbell SL, Burridge K. Direct activation of RhoA by reactive oxygen species requires a redox-sensitive motif. PLoS One 2009;4:e8045.

ABSTRACT (IN KOREAN)

국소 분절 사구체 경화증에서 사구체 지질 축적 및 신장 손상에 대한 ABCA1의 역할

< 지 도 교 수 강 신 욱 >

연세대학교 대학원 의과학과

박 지 민

배경: 사구체 지질 축적은 국소 분절 사구체 경화증 (FSGS)의 병리학적 특징 중 하나이다. 최근 보고에 의하면 ATP 결합 카세트 수송체 A1 (ABCA1)이 세포 지질 항상성에 중요한 역할을 담당하는 것으로 알려지고 있고 다양한 신질환 모델에서 ABCA1의 이상이 사구체 기질 축적에 관여하는 것으로 알려져 있다.

목적: 따라서, 본 연구를 통하여 국소 분절 사구체 경화증 (FSGS) 모델을 통해 사구체 및 족세포의 지질 축적과 손상 과정에서 ABCA1이 어떠한 역할을 하는지 알아보고자 하였다.

방법: 사람의 신장 생검 샘플을 이용하여 FSGS 환자에서 사구체에서 ABCA1의 mRNA 발현을 분석하였다. 세포 실험에서 배양 족세포에 Adriamycin (ADR)과 TNF-α를 이용하여 자극하였다. ABCA1 발현을 상향 조절하기 위해 LXR-α agonist인 GW683965를 처리하였다. FSGS 동물 모델을 만들기 위해, C57BL/6 및 족세포 특이적 ABCA1 KO 마우스에 25mg/kg의 ADR를 정맥내 투여하였고, GW683965는 ADR을 처리한 BALB/C 마우스에 삼투압 펌프를 통해 투여하였다.

실험동물에서 단백뇨와 신장조직에서 콜레스테롤 및 트리글리세리드 수치를 측정하였다. 활성 RhoA 염색 및 BODIPY493/503 염색을 통해 사구체내 콜레스테롤 침착을 확인하였다. 세포 사멸, 미토콘드리아 손상 관련 인자는 세포와 실험 동물에서 각각 분석하였다.

결과: 대조군과 비교하여, FSGS환자의 신장과 FSGS 동물 모델에서 ABCA1의 발현이 의미있게 감소 하였다. 그리고, FSGS 마우스에 비하여 족세포 특이적 ABCA1 KO FSGS 마우스의 신장에서 사구체의 알부민뇨, 콜레스테롤 및 중성지방이 모두 의미있게 증가되었고, 전자현미경 검사에서 족돌기 소실이 유의하게 증가되었다. 또한, FSGS군에서 사구체내 활성 RhoA가 증가하였으며, 미토콘드리아 구조 변화와 지방산 산화 장애 및 에너지 대사 효소 이상은 ADR으로 처리한 족세포 특이적 ABCA1 KO 쥐의 신장에서 wild type FSGS 마우스에 비해 훨씬 악화되었다.

ABCA1 발현을 증가시켜주는 GW683965를 처리하였을 때, FSGS군에서 증가되었던 알부민뇨, 콜레스테롤 및 중성지방 축적, 그리고 족돌기 융합이 완화되었으며, 활성 RhoA가 저해되었고 미토콘드리아의 구조 변화 및 지방산 산화 장애, 세포사멸이 의미있게 개선되었다. ADR 및 TNF-α로 처리한 족세포에서 세포 내 지질 축적이 증가하였으며, 세포사멸 및 미토콘드리아 기능 장애가 증가하였고 이러한 이상 소견은 ABCA1 agonist인 GW683965 처리를 통해 완화되었다.

결론: 이상의 결과로, 국소 분절 사구체 경화증에서 ABCA1이 사구체 지질 축적 및 족세포 손상에 중요한 역할을 하며, 약물을 통해

ABCA1의 활성을 증가시키는 것이 국소 분절 사구체 경화증의 치료에 유용할 것으로 사료된다.

핵심되는 말: ABCA1, 지질 축적, 족세포, 미토콘드리아, 국소 분절 사구체 경화증